

# Dilated convolution with learnable spacings

**Ismail Khalfaoui Hassani**  
ANITI  
Université de Toulouse  
France  
ismail.khalfaoui-hassani@univ-tlse3.fr

**Thomas Pellegrini**  
IRIT, CNRS  
Université de Toulouse  
France  
thomas.pellegrini@irit.fr

**Timothée Masquelier**  
CerCo UMR 5549, CNRS  
Université de Toulouse  
France  
timothee.masquelier@cnrs.fr

Dilated convolution is basically a convolution with a wider kernel created by regularly inserting spaces between the kernel elements. In this article, we present a new version of the dilated convolution in which the spacings are made learnable via backpropagation through an interpolation technique. We call this method “Dilated Convolution with Learnable Spacings” (DCLS) and we generalize its approach to the  $n$ -dimensional convolution case. However, our main focus here will be the 2D case for which we developed two implementations: a naive one that constructs the dilated kernel, suitable for small dilation rates, and a more time/memory efficient one that uses a modified version of the “im2col” algorithm. We then illustrate how this technique improves the accuracy of existing architectures on semantic segmentation task on Pascal Voc 2012 dataset via a simple drop-in replacement of the classical dilated convolutional layers by DCLS ones. Furthermore, we show that DCLS allows to reduce the number of learnable parameters of the depthwise convolutions used in the recent ConvMixer architecture by a factor 3 with no or very low reduction in accuracy and that by replacing large dense kernels with sparse DCLS ones. The code of the method is based on Pytorch and available at: <https://github.com/K-H-Ismail/Dilated-Convolution-with-Learnable-Spacings-PyTorch>.

## 1 Introduction

The receptive field of a deep convolutional network is a crucial element to take into account when it comes to recognition and segmentation tasks in computer vision. For instance, a logarithmic relationship between classification accuracy and receptive field size has been observed in [1]. This tells us that large receptive fields are necessary for high-level vision tasks, but with logarithmically diminishing rewards and thus more computational cost to reach them.

One of the approaches that successfully manages to

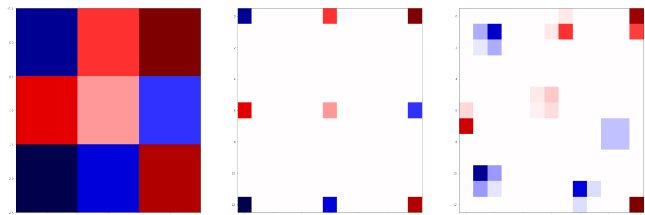


Fig. 1. From left to right: a regular  $3 \times 3$  kernel, a dilated  $3 \times 3$  kernel and a Dcls2d  $3 \times 3$  kernel in which the  $(x, y)$  position of each weight is learnable.

inflate the receptive field of a convolutional layer without adding extra learnable parameters is called dilated convolution. Dilated convolution or “atrous convolution” was first described in [2] and [3] under the name “convolution with a dilated filter” before referring to it as “dilated convolution” in [4]. The purpose of this approach is to inflate the convolutional kernel by regularly inserting spaces between the kernel elements as depicted in Figure 1. The spacing between elements is thus constant, it is a hyper-parameter usually referred to as “dilation” or “dilation rate”.

Several approaches for learning arbitrary geometric changes within the convolutional kernel have emerged, such as [5] and [6]. Those techniques aim to reshape the receptive fields in a way that filters can capture fine object differences such as varied sizes and irregular forms. These approaches are often quite efficient since they do not require any intermediate pre-processing of picture data to encode invariant features [7].

In this context, we developed DCLS (Dilated Convolution with Learnable Spacings) which is a new convolution method. In DCLS, the positions of the weights within the convolutional kernel are learned in a gradient-based manner, and the inherent problem of non-differentiability due to the

integer nature of the positions in the kernel is solved by using an interpolation method. DCLS comes in six sub-versions: 1D, 2D, 3D and what we call N-MD methods, namely: “2-1D, 3-1D and 3-2D” where a N-dimension kernel is used but spacings are learned only along M dimension(s). The main focus of this paper will be the 2D version for which we detail mathematical proofs and implementation specificities.

## 2 Related work

### 2.1 Effective receptive field

The work that mainly motivated the DCLS method is that of [8] which characterizes how much each input pixel in a receptive field can impact the output of a unit in the downstream convolutional layers of a neural network, leading to the notion of an effective receptive field. Among the findings of this work the most relevant ones for ours are:

Not all pixels in a receptive field contribute equally to an output response.

The kernel center have much larger impact. In fact, the effective receptive field has a centered Gaussian distribution.

Given these findings, introducing a new degree of freedom by learning the positions of non-zero weights in dilated kernels might increase the expressive power of convolutional neural networks.

### 2.2 Deformable convolution

The work that relates the most to DCLS is that of deformable convolutions [6] where offsets from the regular dilated grid are optimized. Deformable convolutions turned to be effective for sophisticated vision tasks such as object detection and semantic segmentation. Nevertheless, DCLS is different from it in several ways:

Deformable convolutions require the application of a regular convolution to get the offsets that are then passed to the actual deformable method. Conversely, in DCLS-construct method, a dilated kernel with learnable spacings is constructed and then passed to the convolution operation. In DCLS-im2col method, no kernel construction is required as the convolution is done intrinsically by the “im2col” algorithm and the matrix-matrix multiplication.

Due to the last fact, the number of extra learnable parameters in 2D deformable convolutions (in addition to kernel weights) is the number of kernel elements in the preliminary convolution, precisely  $(\text{channels\_in}, 2 * K\_H * K\_W, K\_H, K\_W)$  with  $K\_H$  and  $K\_W$  being the kernel height and width, which establishes a strong dependence between the offsets and the input feature map. Contrarily, in 2D-DCLS-construct, the number of extra parameters dedicated to learning positions is simply twice the number of kernel weights  $(2, \text{channels\_out}, \text{channels\_in}, K\_H, K\_W)$ , which makes them independent from the feature map. However, in 2D-DCLS-im2col, only  $(2,$

$\text{channels\_in}, K\_H, K\_W)$  extra parameters are required as applying im2col algorithm with more parameters turns out to be computationally prohibitive (this will be detailed in Section 4).

Finally, in order to solve the fundamental problem of magnitude discrepancy between positions and their gradients in DCLS, we use a scaling technique that will be described in Section 5 and that allows us to have a common learning rate for all learnable parameters. Conversely, in deformable convolutions the learning rates of the offsets are set independently of the standard ones.

## 3 DCLS-construct: DCLS with kernel construction

In the following, we show how to mathematically describe the DCLS kernel construction and how to explicitly calculate the gradients of the loss function with respect to weights and positions that are used in the backpropagation algorithm.

### 3.1 Notation and preliminaries

We denote by  $\lfloor \cdot \rfloor$  the floor function and we define its derivative by the zero function.

$$\forall x \in \mathbb{R}, \lfloor x \rfloor' \stackrel{\text{def}}{=} 0 \quad (1)$$

We denote respectively by  $m, n \in \mathbb{N}^* \times \mathbb{N}^*$  the dimensions of the weights along the x-axis and the y-axis and by  $d_1, d_2 \in \mathbb{N}^* \times \mathbb{N}^*$  the maximum dilations for the constructed kernel. The dimension of the constructed kernel is thus  $m.d_1 \times n.d_2$ .

The  $m \times n$  matrix space over  $\mathbb{R}$  is defined as the set of all  $m \times n$  matrices over  $\mathbb{R}$ , and is denoted  $\mathcal{M}_{m,n}(\mathbb{R})$ .

The Frobenius inner product  $\times_F$  of two matrices  $A$  and  $B$  of  $\mathcal{M}_{m,n}(\mathbb{R})$  is defined by:

$$A \times_F B = \text{tr}(A^T B)$$

Lowercase  $w, p^1$  and  $p^2$  respectively stand for the weight, the position of that weight along the x-axis (width) and its position along the y-axis (height) in the scalar case while uppercase  $W = (w_{i,j})_{1 \leq i \leq m, 1 \leq j \leq n}$ ,  $P^1 = (p^1_{i,j})_{1 \leq i \leq m, 1 \leq j \leq n}$  and  $P^2 = (p^2_{i,j})_{1 \leq i \leq m, 1 \leq j \leq n}$  respectively stand for the weight, the width-position of that weight and its height-position in the matrix case.

The proofs and algorithms that will be shown in the next sections are made for the case of tensors with one input channel and one output channel. Without loss of generality, those proofs and algorithms hold for the general case of 4D tensors by considering and applying them channel-wise.

### 3.2 2D-DCLS, scalar weight case

We begin by the case of a kernel containing only one weight (instead of the 9 weights shown in Fig. 1).

The function  $f$  that defines the kernel construction in the scalar weight case is as follows:

$$f: \mathbb{R} \times \mathbb{R} \times \mathbb{R} \rightarrow \mathcal{M}_{md_1, nd_2}(\mathbb{R}) \quad (2)$$

$$w, p^1, p^2 \mapsto K$$

where  $\forall i \in \llbracket 1 \dots md_1 \rrbracket, \forall j \in \llbracket 1 \dots nd_2 \rrbracket$ :

$$K_{ij} = \begin{cases} w(1-r^1)(1-r^2) & \text{if } i = \lfloor p^1 \rfloor, j = \lfloor p^2 \rfloor \\ w r^1 (1-r^2) & \text{if } i = \lfloor p^1 \rfloor + 1, j = \lfloor p^2 \rfloor \\ w(1-r^1)r^2 & \text{if } i = \lfloor p^1 \rfloor, j = \lfloor p^2 \rfloor + 1 \\ w r^1 r^2 & \text{if } i = \lfloor p^1 \rfloor + 1, j = \lfloor p^2 \rfloor + 1 \\ 0 & \text{else} \end{cases} \quad (3)$$

and where the fractional parts are:

$$\begin{aligned} r^1 &= \{p^1\} = p^1 - \lfloor p^1 \rfloor \\ r^2 &= \{p^2\} = p^2 - \lfloor p^2 \rfloor \end{aligned} \quad (4)$$

The constructed kernel  $K$  is zero except for at most the 4 adjacent positions that represent the 2D interpolation of the single weight  $w$ . We then define the scalar loss function as

$$loss = g(f(w, p^1, p^2)) \quad (5)$$

with  $g: \mathcal{M}_{md_1, nd_2}(\mathbb{R}) \rightarrow \mathbb{R}$  a differentiable function that models the action of all the layers that will follow  $f$  in the model.

By applying the chain rule we obtain

$$\frac{\partial loss}{\partial w} = g'(f(w, p^1, p^2)) \times_{\mathbb{F}} \frac{\partial f(w, p^1, p^2)}{\partial w} \quad (6)$$

$$\frac{\partial loss}{\partial p^1} = g'(f(w, p^1, p^2)) \times_{\mathbb{F}} \frac{\partial f(w, p^1, p^2)}{\partial p^1} \quad (7)$$

$$\frac{\partial loss}{\partial p^2} = g'(f(w, p^1, p^2)) \times_{\mathbb{F}} \frac{\partial f(w, p^1, p^2)}{\partial p^2} \quad (8)$$

with

$$\begin{aligned} g'(f(w, p^1, p^2)) &= \frac{\partial loss}{\partial K} \\ &= \frac{\partial loss}{\partial f(w, p^1, p^2)} \end{aligned} \quad (9)$$

Let us put

$$g'(f(w, p^1, p^2)) = G = \begin{bmatrix} g_{11} & g_{12} & \cdots & g_{1nd_2} \\ g_{21} & \ddots & & g_{1md_1} \\ \vdots & & \ddots & \vdots \\ g_{md_1 1} & g_{12} & \cdots & g_{md_1 nd_2} \end{bmatrix} \quad (10)$$

and let us consider two column vectors  $X = [x_1 \ x_2 \ \cdots \ x_{md_1}]^T$  of  $\mathbb{R}^{md_1}$  and  $Y = [y_1 \ y_2 \ \cdots \ y_{nd_2}]^T$  of  $\mathbb{R}^{nd_2}$ . We have:

$$X^T f(w, p^1, p^2) Y = \sum_{i=1}^{md_1} \sum_{j=1}^{nd_2} K_{ij} x_i y_j \quad (11)$$

Since  $K$  is zero except for the 4 aforementioned positions, we have

$$\begin{aligned} X^T f(w, p^1, p^2) Y &= K_{\lfloor p^1 \rfloor \lfloor p^2 \rfloor} x_{\lfloor p^1 \rfloor} y_{\lfloor p^2 \rfloor} \\ &+ K_{\lfloor p^1 \rfloor + 1 \lfloor p^2 \rfloor} x_{\lfloor p^1 \rfloor + 1} y_{\lfloor p^2 \rfloor} \\ &+ K_{\lfloor p^1 \rfloor \lfloor p^2 \rfloor + 1} x_{\lfloor p^1 \rfloor} y_{\lfloor p^2 \rfloor + 1} \\ &+ K_{\lfloor p^1 \rfloor + 1 \lfloor p^2 \rfloor + 1} x_{\lfloor p^1 \rfloor + 1} y_{\lfloor p^2 \rfloor + 1} \end{aligned} \quad (12)$$

By deriving this expression with respect to  $w, p^1$  and  $p^2$  we obtain

$$\begin{aligned} \frac{\partial (X^T f(w, p^1, p^2) Y)}{\partial w} &= (1-r^1)(1-r^2) x_{\lfloor p^1 \rfloor} y_{\lfloor p^2 \rfloor} \\ &+ r^1(1-r^2) x_{\lfloor p^1 \rfloor + 1} y_{\lfloor p^2 \rfloor} \\ &+ (1-r^1)r^2 x_{\lfloor p^1 \rfloor} y_{\lfloor p^2 \rfloor + 1} \\ &+ r^1 r^2 x_{\lfloor p^1 \rfloor + 1} y_{\lfloor p^2 \rfloor + 1} \end{aligned} \quad (13)$$

$$\begin{aligned} \frac{\partial (X^T f(w, p^1, p^2) Y)}{\partial p^1} &= w [-(1-r^2) x_{\lfloor p^1 \rfloor} y_{\lfloor p^2 \rfloor} \\ &+ (1-r^2) x_{\lfloor p^1 \rfloor + 1} y_{\lfloor p^2 \rfloor} \\ &- r^2 x_{\lfloor p^1 \rfloor} y_{\lfloor p^2 \rfloor + 1} \\ &+ r^2 x_{\lfloor p^1 \rfloor + 1} y_{\lfloor p^2 \rfloor + 1}] \end{aligned} \quad (14)$$

$$\begin{aligned} \frac{\partial (X^T f(w, p^1, p^2) Y)}{\partial p^2} &= w [-(1-r^1) x_{\lfloor p^1 \rfloor} y_{\lfloor p^2 \rfloor} \\ &- r^1 x_{\lfloor p^1 \rfloor + 1} y_{\lfloor p^2 \rfloor} \\ &+ (1-r^1) x_{\lfloor p^1 \rfloor} y_{\lfloor p^2 \rfloor + 1} \\ &+ r^1 x_{\lfloor p^1 \rfloor + 1} y_{\lfloor p^2 \rfloor + 1}] \end{aligned} \quad (15)$$

Because of the linearity of the differentiation in the three previous equations, we could write:

$$\frac{\partial (X^T f(w, p^1, p^2) Y)}{\partial w} = X^T \frac{\partial f(w, p^1, p^2)}{\partial w} Y = X^T G_w Y \quad (16)$$

$$\frac{\partial (X^T f(w, p^1, p^2) Y)}{\partial p^1} = X^T \frac{\partial f(w, p^1, p^2)}{\partial p^1} Y = X^T G_{p^1} Y \quad (17)$$

$$\frac{\partial (X^T f(w, p^1, p^2) Y)}{\partial p^2} = X^T \frac{\partial f(w, p^1, p^2)}{\partial p^2} Y = X^T G_{p^2} Y \quad (18)$$

where  $G_w, G_{p^1}, G_{p^2}$ , respectively stand for the  $md_1$  by  $nd_2$  matrices described below and which have zeros everywhere

except at the four positions of interpolation.

$$G_w = \begin{pmatrix} 0 & \dots & \lfloor p^2 \rfloor & \lfloor p^2 \rfloor + 1 & \dots & 0 \\ \vdots & \ddots & 0 & 0 & \ddots & \vdots \\ 0 & 0 & (1-r^1)(1-r^2) & r^2(1-r^1) & 0 & 0 \\ 0 & 0 & r^1(1-r^2) & r^1 r^2 & 0 & 0 \\ \vdots & \ddots & 0 & 0 & \ddots & \vdots \\ 0 & \dots & 0 & 0 & \dots & 0 \end{pmatrix} \begin{matrix} \lfloor p^1 \rfloor \\ \lfloor p^1 \rfloor + 1 \end{matrix} \quad (19)$$

$$G_{p^1} = \begin{pmatrix} 0 & \dots & \lfloor p^2 \rfloor & \lfloor p^2 \rfloor + 1 & \dots & 0 \\ \vdots & \ddots & 0 & 0 & \ddots & \vdots \\ 0 & 0 & -w(1-r^2) & -wr^2 & 0 & 0 \\ 0 & 0 & w(1-r^2) & wr^2 & 0 & 0 \\ \vdots & \ddots & 0 & 0 & \ddots & \vdots \\ 0 & \dots & 0 & 0 & \dots & 0 \end{pmatrix} \begin{matrix} \lfloor p^1 \rfloor \\ \lfloor p^1 \rfloor + 1 \end{matrix} \quad (20)$$

$$G_{p^2} = \begin{pmatrix} 0 & \dots & \lfloor p^2 \rfloor & \lfloor p^2 \rfloor + 1 & \dots & 0 \\ \vdots & \ddots & 0 & 0 & \ddots & \vdots \\ 0 & 0 & -w(1-r^1) & w(1-r^1) & 0 & 0 \\ 0 & 0 & -wr^1 & wr^1 & 0 & 0 \\ \vdots & \ddots & 0 & 0 & \ddots & \vdots \\ 0 & \dots & 0 & 0 & \dots & 0 \end{pmatrix} \begin{matrix} \lfloor p^1 \rfloor \\ \lfloor p^1 \rfloor + 1 \end{matrix} \quad (21)$$

From the three equations (16), (17) and (18), we can identify

$$\frac{\partial f(w, p^1, p^2)}{\partial w} = G_w \quad (22)$$

$$\frac{\partial f(w, p^1, p^2)}{\partial p^1} = G_{p^1} \quad (23)$$

$$\frac{\partial f(w, p^1, p^2)}{\partial p^2} = G_{p^2} \quad (24)$$

Finally, we have

$$\frac{\partial loss}{\partial w} = G_{\mathbb{F}} \times G_w = (1-r^1)(1-r^2) g_{\lfloor p^1 \rfloor \lfloor p^2 \rfloor} + r^1(1-r^2) g_{\lfloor p^1 \rfloor + 1 \lfloor p^2 \rfloor} + (1-r^1)r^2 g_{\lfloor p^1 \rfloor \lfloor p^2 \rfloor + 1} + r^1 r^2 g_{\lfloor p^1 \rfloor + 1 \lfloor p^2 \rfloor + 1} \quad (25)$$

$$\frac{\partial loss}{\partial p^1} = G_{\mathbb{F}} \times G_{p^1} = w[-(1-r^2) g_{\lfloor p^1 \rfloor \lfloor p^2 \rfloor} + (1-r^2) g_{\lfloor p^1 \rfloor + 1 \lfloor p^2 \rfloor} - r^2 g_{\lfloor p^1 \rfloor \lfloor p^2 \rfloor + 1} + r^2 g_{\lfloor p^1 \rfloor + 1 \lfloor p^2 \rfloor + 1}] \quad (26)$$

$$\frac{\partial loss}{\partial p^2} = G_{\mathbb{F}} \times G_{p^2} = w[-(1-r^1) g_{\lfloor p^1 \rfloor \lfloor p^2 \rfloor} - r^1 g_{\lfloor p^1 \rfloor + 1 \lfloor p^2 \rfloor} + (1-r^1) g_{\lfloor p^1 \rfloor \lfloor p^2 \rfloor + 1} + r^1 g_{\lfloor p^1 \rfloor + 1 \lfloor p^2 \rfloor + 1}] \quad (27)$$

### 3.3 2D-DCLS, general case

The general case is the one where the weights  $W$  and the positions  $P^1, P^2$  are stored in 2D matrices. The function  $f$  defined in equation (2) is then extended to the function  $F$  defined as follows:

$$F: (\mathcal{M}_{m,n}(\mathbb{R}))^3 \rightarrow \mathcal{M}_{md_1, nd_2}(\mathbb{R}) \quad (28)$$

$$W, P^1, P^2 \mapsto K$$

where

$$K = \sum_{i=1}^m \sum_{j=1}^n f(w_{i,j}, p_{i,j}^1, p_{i,j}^2) \quad (29)$$

The constructed kernel  $K$  here is the result of a double summation of the function  $f$  defined in (2) over the elements of weight and position matrices. We then define the scalar loss function as in (5).

As the summations in (29) are independent and by the linearity of the differentiation, we deduce from (25), (26) and (27) the gradients of the loss function with respect to weights and positions in the general case:

$\forall i \in \llbracket 1 \dots m \rrbracket, \forall j \in \llbracket 1 \dots n \rrbracket :$

$$\begin{aligned} \left( \frac{\partial \text{loss}}{\partial W} \right)_{i,j} &= (1 - r_{i,j}^1) (1 - r_{i,j}^2) g_{\lfloor p_{i,j}^1 \rfloor \lfloor p_{i,j}^2 \rfloor} \\ &\quad + r_{i,j}^1 (1 - r_{i,j}^2) g_{\lfloor p_{i,j}^1 \rfloor + 1 \lfloor p_{i,j}^2 \rfloor} \\ &\quad + (1 - r_{i,j}^1) r_{i,j}^2 g_{\lfloor p_{i,j}^1 \rfloor \lfloor p_{i,j}^2 \rfloor + 1} \\ &\quad + r_{i,j}^1 r_{i,j}^2 g_{\lfloor p_{i,j}^1 \rfloor + 1 \lfloor p_{i,j}^2 \rfloor + 1} \end{aligned} \quad (30)$$

$$\begin{aligned} \left( \frac{\partial \text{loss}}{\partial P^1} \right)_{i,j} &= w_{i,j} [ - (1 - r_{i,j}^2) g_{\lfloor p_{i,j}^1 \rfloor \lfloor p_{i,j}^2 \rfloor} \\ &\quad + (1 - r_{i,j}^2) g_{\lfloor p_{i,j}^1 \rfloor + 1 \lfloor p_{i,j}^2 \rfloor} \\ &\quad - r_{i,j}^2 g_{\lfloor p_{i,j}^1 \rfloor \lfloor p_{i,j}^2 \rfloor + 1} \\ &\quad + r_{i,j}^2 g_{\lfloor p_{i,j}^1 \rfloor + 1 \lfloor p_{i,j}^2 \rfloor + 1} ] \end{aligned} \quad (31)$$

$$\begin{aligned} \left( \frac{\partial \text{loss}}{\partial P^2} \right)_{i,j} &= w_{i,j} [ - (1 - r_{i,j}^1) g_{\lfloor p_{i,j}^1 \rfloor \lfloor p_{i,j}^2 \rfloor} \\ &\quad - r_{i,j}^1 g_{\lfloor p_{i,j}^1 \rfloor + 1 \lfloor p_{i,j}^2 \rfloor} \\ &\quad + (1 - r_{i,j}^1) g_{\lfloor p_{i,j}^1 \rfloor \lfloor p_{i,j}^2 \rfloor + 1} \\ &\quad + r_{i,j}^1 g_{\lfloor p_{i,j}^1 \rfloor + 1 \lfloor p_{i,j}^2 \rfloor + 1} ] \end{aligned} \quad (32)$$

### 3.4 Forward and backward algorithms for 2D-DCLS with kernel construction

In the following, we describe with pseudocode the forward and backward passes for kernel construction used in 2D-DCLS. In practice,  $W$ ,  $P^1$  and  $P^2$  are 4-D tensors of size (channels\_out, channels\_in // groups, K\_H, K\_W), but the algorithms presented here are easily extended to this case by applying them channel-wise. The weights and positions are randomly initialized, then positions are centered and clamped to match positive indices.

---

#### Algorithm 1 2D-DCLS kernel construction forward pass

---

**Input:**  $W, P^1, P^2$  : tensors of dimension  $m \times n$

**Output:**  $K$  : the constructed kernel

```

1:  $K \leftarrow 0$ 
2:  $p^1 \leftarrow \lfloor P^1 \rfloor; \quad p^2 \leftarrow \lfloor P^2 \rfloor$ 
3:  $R^1 \leftarrow P^1 - p^1; \quad R^2 \leftarrow P^2 - p^2$ 
4: save_for_backward ( $p^1, p^2, R^1, R^2$ )
5: for  $i = 0 \rightarrow m - 1$  do
6:   for  $j = 0 \rightarrow n - 1$  do
7:      $K[p_{i,j}^1, p_{i,j}^2] \leftarrow W_{ij} * (1 - R_{ij}^1) * (1 - R_{ij}^2)$ 
8:      $K[p_{i,j}^1 + 1, p_{i,j}^2] \leftarrow W_{ij} * (R_{ij}^1) * (1 - R_{ij}^2)$ 
9:      $K[p_{i,j}^1, p_{i,j}^2 + 1] \leftarrow W_{ij} * (1 - R_{ij}^1) * (R_{ij}^2)$ 
10:     $K[p_{i,j}^1 + 1, p_{i,j}^2 + 1] \leftarrow W_{ij} * (R_{ij}^1) * (R_{ij}^2)$ 
11:   end for
12: end for

```

---



---

#### Algorithm 2 2D-DCLS kernel construction backward pass

---

**Input:**  $\text{Grad}K = \frac{\partial \text{Loss}}{\partial K}$  : tensor of dimension  $m.d_1 \times n.d_2$

**Output:**  $\frac{\partial \text{Loss}}{\partial W}, \frac{\partial \text{Loss}}{\partial P^1}, \frac{\partial \text{Loss}}{\partial P^2}$  : tensors of dimension  $m \times n$

```

1:  $\frac{\partial \text{Loss}}{\partial W} \leftarrow 0, \frac{\partial \text{Loss}}{\partial P^1} \leftarrow 0, \frac{\partial \text{Loss}}{\partial P^2} \leftarrow 0$ 
2:  $p^1, p^2, R^1, R^2 \leftarrow \text{load\_saved}()$ 
3: for  $i = 0 \rightarrow m - 1$  do
4:   for  $j = 0 \rightarrow n - 1$  do
5:

```

$$\begin{aligned} \frac{\partial \text{Loss}}{\partial W}[i, j] &\leftarrow \frac{\partial \text{Loss}}{\partial K}[p_{i,j}^1, p_{i,j}^2] * (1 - R_{ij}^1) * (1 - R_{ij}^2) \\ &\quad + \frac{\partial \text{Loss}}{\partial K}[p_{i,j}^1 + 1, p_{i,j}^2] * R_{ij}^1 * (1 - R_{ij}^2) \\ &\quad + \frac{\partial \text{Loss}}{\partial K}[p_{i,j}^1, p_{i,j}^2 + 1] * (1 - R_{ij}^1) * R_{ij}^2 \\ &\quad + \frac{\partial \text{Loss}}{\partial K}[p_{i,j}^1 + 1, p_{i,j}^2 + 1] * R_{ij}^1 * R_{ij}^2 \end{aligned}$$

6:

$$\begin{aligned} \frac{\partial \text{Loss}}{\partial P^1}[i, j] &\leftarrow - \frac{\partial \text{Loss}}{\partial K}[p_{i,j}^1, p_{i,j}^2] * W_{ij} * (1 - R_{ij}^2) \\ &\quad + \frac{\partial \text{Loss}}{\partial K}[p_{i,j}^1 + 1, p_{i,j}^2] * W_{ij} * (1 - R_{ij}^2) \\ &\quad - \frac{\partial \text{Loss}}{\partial K}[p_{i,j}^1, p_{i,j}^2 + 1] * W_{ij} * R_{ij}^2 \\ &\quad + \frac{\partial \text{Loss}}{\partial K}[p_{i,j}^1 + 1, p_{i,j}^2 + 1] * W_{ij} * R_{ij}^2 \end{aligned}$$

7:

$$\begin{aligned} \frac{\partial \text{Loss}}{\partial P^2}[i, j] &\leftarrow - \frac{\partial \text{Loss}}{\partial K}[p_{i,j}^1, p_{i,j}^2] * W_{ij} * (1 - R_{ij}^1) \\ &\quad - \frac{\partial \text{Loss}}{\partial K}[p_{i,j}^1 + 1, p_{i,j}^2] * W_{ij} * R_{ij}^1 \\ &\quad + \frac{\partial \text{Loss}}{\partial K}[p_{i,j}^1, p_{i,j}^2 + 1] * W_{ij} * (1 - R_{ij}^1) \\ &\quad + \frac{\partial \text{Loss}}{\partial K}[p_{i,j}^1 + 1, p_{i,j}^2 + 1] * W_{ij} * R_{ij}^1 \end{aligned}$$

8: **end for**

9: **end for**

---

The nested for loops in the algorithms are fully parallelized using GPU threads. The 2D-DCLS convolution with kernel construction is then obtained by applying the classical 2D-convolution using the constructed kernel.

## 4 DCLS-im2col: 2D-DCLS with an im2col algorithm

Despite its ease to be described and implemented, the constructive DCLS method presents a performance problem when moving to larger dilations. Indeed, the constructed kernel is largely sparse (it has a sparsity of  $1 - \frac{1}{d_1 d_2}$ ) and the zeros are effectively taken into account during the convolution leading to great losses of performance in time and memory as shown in Figure 2 and this all the more as the dilation is large.

This is why we implemented an alternative method by adapting the im2col algorithm [9] which aims to speed up

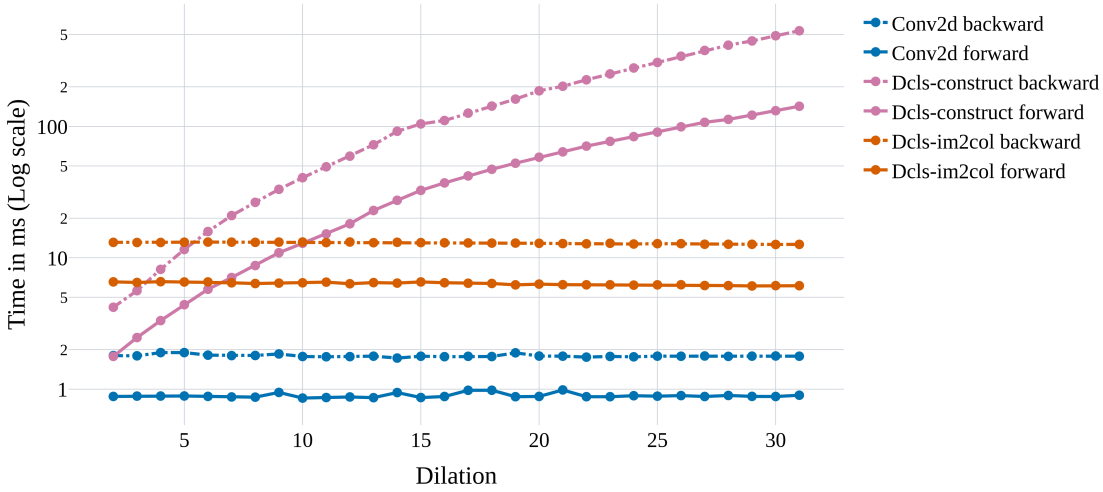


Fig. 2. Evolution of computation time for cuDNN Conv2d, Dcls2d-construct and Dcls2d-im2col as functions of the dilation rate.

the convolution by unrolling the input into a Toeplitz matrix and then performing matrix multiplication.

In the forward pass for instance, an input of size  $(\text{channels\_in}, H_{\text{in}}, W_{\text{in}})$  is unrolled into a  $(\text{channels\_in} * K_h * K_w, H_{\text{out}} * W_{\text{out}})$  matrix (this is the im2col algorithm), weights are then reshaped into a  $(\text{channels\_out}, \text{channels\_in} * K_h * K_w)$  matrix before multiplying the two, which gives the output result of the forward convolution. A similar procedure is applied in the backward pass in order to get the gradient with respect to the weights.

Similarly, the DCLS-im2col algorithm unrolls the input image but adds the interpolation positions leading to a  $(4 * \text{channels\_in} * K_h * K_w, H_{\text{out}} * W_{\text{out}})$  matrix where the 4 factor represents the 2D interpolation. The weights are also interpolated as in Algorithm (1) and reshaped into a  $(\text{channels\_out}, 4 * \text{channels\_in} * K_h * K_w)$  matrix before multiplying the two. The backward pass is slightly different as we compute, additionally to the gradients of weights, those of the positions where a reduction is made over output channels.

A limitation of the DCLS-im2col method compared to the constructive one is that it turns out to be computationally prohibitive to have  $(2, \text{channels\_out}, \text{channels\_in}, K_h, K_w)$  learnable positions in the im2col algorithm and furthermore in the matrix multiplication that follows as it becomes a tensor product. Therefore, we force all the output channels to have the same positions, leading to a position tensor of size  $(2, \text{channels\_in}, K_H, K_W)$ .

Taking all this into consideration, we obtain a competitive method in terms of time and memory as shown in Figure 3. More implementation details are to be found in the repository mentioned in the abstract.

## 5 Scaling

From equation (30) we see that the norm of the gradient of the weights has the same magnitude as the norm of the

gradient of the output:

$$\left\| \frac{\partial \text{loss}}{\partial W} \right\| \sim \left\| g'(F(W, P^1, P^2)) \right\| \quad (33)$$

while equations (31) and (32) reveal that the norms of the gradients of the positions have the same magnitude as the norm of the gradient of the output times the norm of the weights.

$$\left\| \frac{\partial \text{loss}}{\partial P^1} \right\| \sim \left\| \frac{\partial \text{loss}}{\partial P^2} \right\| \sim \left\| g'(F(W, P^1, P^2)) \right\| \cdot \|W\| \quad (34)$$

The latter equation raises a fundamental observation : there is a magnitude discrepancy between positions (which are typically of magnitude  $(10^0 \sim 10^1)$  and their gradients (of magnitude equal to the square of weights magnitude  $10^{-4} \sim 10^{-5}$ ).

One way to solve this problem is to assign tailored learning rates to the position parameters during learning process (as it is not homogeneous to use the same learning rates for the weights and the positions, given that they have different units). Alternatively, we can scale the gradients and use a common learning rate. We chose this option for simplicity.

The scaling technique used here is inspired by Xavier [10] and Kaiming [11] initializations, and it is basically a multiplicative variable change applied on position tensors. We define the scaling used for  $P^1$  and  $P^2$  as

$$\text{scaling} = \text{gain} \sqrt{\text{in\_channels} \cdot \text{kernel\_h} \cdot \text{kernel\_w}} \quad (35)$$

where the gain is a hyperparameter that can be fine tuned by the user.

By variable change the two position tensors become

$$P_s^1 = \frac{P^1}{\text{scaling}}, \quad P_s^2 = \frac{P^2}{\text{scaling}} \quad (36)$$

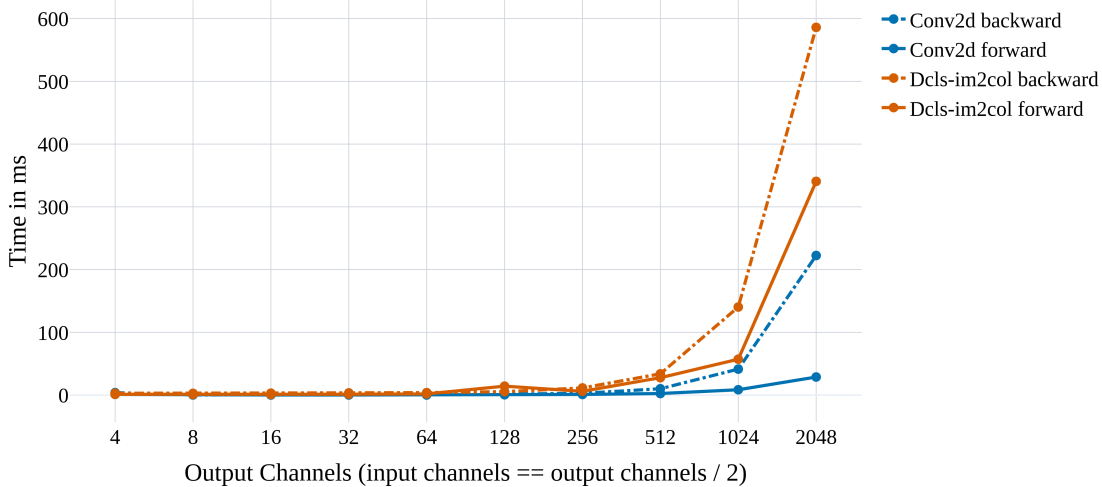


Fig. 3. Evolution of computation time (in ms) for native cuDNN Conv2d and Dcls2d-im2col as functions of output channels.

and we calculate their gradients as

$$\frac{\partial loss}{\partial P_s^1} = \text{scaling} \cdot \frac{\partial loss}{\partial P^1} \quad (37)$$

$$\frac{\partial loss}{\partial P_s^2} = \text{scaling} \cdot \frac{\partial loss}{\partial P^2} \quad (38)$$

This scaling operation is applied at the start of every DCLS-construct and DCLS-im2col method and when needed, the positions  $P^1$  and  $P^2$  can easily be found by re-multiplying by the scaling. The gradients of the positions are multiplied by the scaling in the backward pass as well.

Regarding the positions initialization, we start from the regular grid configuration and we add a random noise for each position in the plan according to a normal law of mean 0 and of standard deviation equal to  $\frac{\text{max\_dilation}}{2 \cdot \text{scaling}}$ .

## 6 Experiments

In this section, we present our experimental results of the 2D-DCLS convolution. Two experiments were conducted: firstly in 6.2, an experiment on CIFAR-10 database using the recent ConvMixer model [12] where we drop-in replaced all the depthwise convolutions of the model by constructive 2D-DCLS ones. Secondly in 6.3, an experiment on Pascal Voc 2012 database using Deeplabv3+ model [13] where we drop-in replaced the 3 dilated convolutions used in the classifier part of that model by 2D-DCLS-im2col ones, we then repeated the same experiment using various backbones pretrained on large image datasets such as ImageNet [13] and Imagenet + COCO + the validation dataset [14] for the Xception65 model [15].

### 6.1 Experimental setup

All our experiments were carried out on a single Quadro RTX 8000 GPU. In order to reproduce our experiments, all

the code and the pretrained models are available in Appendix 8.

### 6.2 CIFAR-10 experiment

The training procedure used in the CIFAR-10 experiment was exactly the same as in [12], we simply replaced the depthwise convolutions used in that model by our constructive DCLS method. The maximum dilation here is 3, thus it is not prohibitive to use DCLS-construct as seen in Figure 2.

We can see from Table 1 that the 2D-DCLS convolution provides better test accuracy than both standard dilated convolution (by +4.4%) and non dilated convolution (by +1.1%) and that with nearly the same number of parameters. Moreover, it reaches slightly lower accuracy than the baseline (by -0.1%) and that with 15% less parameters.

Interestingly enough, the standard dilated convolution achieves much lower performance than DCLS and leads to worse performance than the non dilated  $3 \times 3$  convolution.

Fine-tuning the scaling gain could be profitable, as shown in Table 1 but its effect remains low.

### 6.3 Pascal Voc 2012 validation experiment

For the Pascal Voc experiment, we reconducted the experiments of [13] using Pytorch so as to obtain proper baselines, then we replaced the dilated convolutions used in the classifiers of those baselines by 2D-DCLS-im2col convolutions. We validated this experiment on cropped images of size 513x513 on the Pascal Voc 2012 validation set as described in [13].

We can see from Table 2 that 2D-DCLS-im2col convolution provides better mean IoU than the standard dilated convolution (up to +0.7%) with almost the same number of parameters (less than 0.4% extra parameters) and this independently of the backbone used. The scaling gains used here were roughly tuned and are the same for the three classifier convolutions where DCLS has been used.

Unfortunately, we could not compare to deformable

ConvMixer trained on CIFAR-10.

Width $w$	Depth $d$	Patch Size $p$	Kernel Size $k$	Dilation $d$	Scaling gain	# Params $\times (10^3)$	Method	Acc. (%)
256	16	1	9	1	-	1409	nn.Conv2d	96.74
256	16	1	7	1	-	1278	nn.Conv2d	96.50
256	16	1	3	1	-	1114	nn.Conv2d	95.52
256	16	1	3	3	-	1114	nn.Conv2d	92.21
256	16	1	3	3	$\frac{1}{k\sqrt{w}} \approx 0.02$	<b>1187</b>	Dcls2d	<b>96.51</b>
256	16	1	3	3	$\frac{0.9}{k\sqrt{w}} \approx 0.018$	<b>1187</b>	Dcls2d	<b>96.63</b>

Table 1. Top1 test accuracies on CIFAR-10 trained exactly as in [12].

Deeplabv3+ trained on Pascal Voc 2012.

Backbone	Max Dilation Sizes	Scaling gain	# Params ( $\times 10^6$ )	Method	Mean IoU. (%)	Overall Acc. (%)
MobileNet	[6, 12, 18]	-	5.22	nn.Conv2d	71.79	92.75
MobileNet		10	<b>5.24</b>	Dcls2d	<b>72.57</b>	93.02
ResNet50	[6, 12, 18]	-	39.76	nn.Conv2d	77.70	94.29
ResNet50		4	<b>39.87</b>	Dcls2d	<b>78.43</b>	94.54
ResNet101	[6, 12, 18]	-	58.75	nn.Conv2d	78.71	94.68
ResNet101		4	<b>58.86</b>	Dcls2d	<b>79.42</b>	94.76
Xception65	[6, 12, 18]	-	54.11	nn.Conv2d	86.89	96.81
Xception65		10	<b>54.22</b>	Dcls2d	<b>87.36</b>	96.91

Table 2. Validation mIoU on Pascal Voc 2012 validation set with  $513 \times 513$  crop.

convolutions [6] in this task (mIoU of 75.3% with Resnet101 backbone) as they used an older version of Deeplab [16].

## 7 Limitations

The constructive DCLS method starts to be computationally inefficient for dilation rates greater than 7 as shown in Figure 2. Further investigation will be made to try to implement it using sparse matrix libraries for GPU devices such as cuSparse.

As described in Section 4, the number of learnable parameters of the DCLS-im2col method is reduced by a factor of output channels in order to make it computationally relevant. Still, this method shows good results for large dilations as indicated in Section 6.

The scaling gain introduced in Section 5 is a hyperparameter that should be tuned although the standard scaling could be sufficient in many cases.

DCLS only supports Nvidia CUDA GPU devices for the moment.

## 8 Conclusion

This work proposes a new dilated convolution method where the positions of non-zero kernel elements are made

learnable via backpropagation. We mathematically demonstrated how the gradients of positions could be calculated and we showed two possible implementations for the method. We provided evidence that searching for optimal positions of weights within a dilated kernel could help increase the accuracy of existing architectures with small extra parameters costs. Alternatively, it could reduce the size of large dense kernels used in recent convolutional architectures with a marginal reduction in accuracy.

**Future work.** We would like to investigate how DCLS could make 2D convolution robust towards adversarial attacks. Sparse matrix multiplication could be used to enhance the performance of the constructive DCLS method, we will look into that. Finally, we would like to show that there is an interest in the method also in the 1D and 3D cases.

## References

- [1] Araujo, A., Norris, W., and Sim, J., 2019. “Computing receptive fields of convolutional neural networks”. *Distill*. <https://distill.pub/2019/computing-receptive-fields>.
- [2] Holschneider, M., Kronland-Martinet, R., Morlet, J., and Tchamitchian, P., 1990. “A real-time algorithm for signal analysis with the help of the wavelet transform”. In *Wavelets*. Springer, pp. 286–297.

- [3] Shensa, M. J., 1992. “The discrete wavelet transform: wedding the a trous and mallat algorithms”. *IEEE Trans. Signal Process.*, **40**(10), pp. 2464–2482.
- [4] Yu, F., and Koltun, V., 2015. “Multi-scale context aggregation by dilated convolutions”. *arXiv preprint arXiv:1511.07122*.
- [5] Felzenszwalb, P., McAllester, D., and Ramanan, D., 2008. “A discriminatively trained, multiscale, deformable part model”. In Proc. IEEE/CVF Conf. Comput. Vis. Pattern Recog. (CVPR), IEEE, pp. 1–8.
- [6] Dai, J., Qi, H., Xiong, Y., Li, Y., Zhang, G., Hu, H., and Wei, Y., 2017. “Deformable convolutional networks”. In Proc. IEEE Int. Conf. on Comp. Vision (ICCV), pp. 764–773.
- [7] Mumuni, A., and Mumuni, F., 2021. “Cnn architectures for geometric transformation-invariant feature representation in computer vision: A review”. *SN Computer Science*, **2**(5), pp. 1–23.
- [8] Luo, W., Li, Y., Urtasun, R., and Zemel, R., 2016. “Understanding the effective receptive field in deep convolutional neural networks”. In Proc. Int. Conf. on Neural Information Processing Systems, pp. 4905–4913.
- [9] Chellapilla, K., Puri, S., and Simard, P., 2006. “High Performance Convolutional Neural Networks for Document Processing”. In Proc. Int. Workshop on Frontiers in Handwriting Recognition (IWFHR). <https://hal.inria.fr/inria-00112631>.
- [10] Glorot, X., and Bengio, Y., 2010. “Understanding the difficulty of training deep feedforward neural networks”. In Proc. Int. Conf. on Artificial Intelligence and Statistics, JMLR Workshop and Conference Proceedings, pp. 249–256.
- [11] He, K., Zhang, X., Ren, S., and Sun, J., 2015. “Delving deep into rectifiers: Surpassing human-level performance on imagenet classification”. In Proc. IEEE Int. Conf. on Comp. Vis. (ICCV), pp. 1026–1034.
- [12] Anonymous, 2022. “Patches are all you need?”. In Submitted to The Tenth International Conference on Learning Representations (ICLR). under review.
- [13] Chen, L.-C., Zhu, Y., Papandreou, G., Schroff, F., and Adam, H., 2018. “Encoder-decoder with atrous separable convolution for semantic image segmentation”. In ECCV, pp. 801–818.
- [14] Lin, T.-Y., Maire, M., Belongie, S., Hays, J., Perona, P., Ramanan, D., Dollár, P., and Zitnick, C. L., 2014. “Microsoft coco: Common objects in context”. In ECCV, Springer, pp. 740–755.
- [15] Chollet, F., 2017. “Xception: Deep learning with depthwise separable convolutions”. In Proc. IEEE/CVF Conf. Comput. Vis. Pattern Recog. (CVPR), pp. 1251–1258.
- [16] Chen, L.-C., Papandreou, G., Kokkinos, I., Murphy, K., and Yuille, A. L., 2017. “Deeplab: Semantic image segmentation with deep convolutional nets, atrous convolution, and fully connected CRFs”. *IEEE Trans. on Pattern Analysis and Machine Intelligence*, **40**(4), pp. 834–848.
- [17] Howard, J., 2019. Imagenette. <https://github.com/fastai/imagenette>.
- [18] Deng, J., Dong, W., Socher, R., Li, L.-J., Li, K., and Fei-Fei, L., 2009. “Imagenet: A large-scale hierarchical image database”. In Proc. IEEE/CVF Conf. Comput. Vis. Pattern Recog. (CVPR), IEEE, pp. 248–255.
- [19] Everingham, M., Van Gool, L., Williams, C. K. I., Winn, J., and Zisserman, A., 2012. The PASCAL Visual Object Classes Challenge 2012 (VOC2012) Results. <http://www.pascal-network.org/challenges/VOC/voc2012/workshop/index.html>.
- [20] ICLR 2022 Author, h., 2021. convmixer. <https://github.com/tmp-iclr/convmixer>.
- [21] Gongfan, F., 2019. Deeplabv3plus-pytorch. <https://github.com/VainF/DeepLabV3Plus-Pytorch>.
- [22] Shirh, L., 2021. Xception. <https://github.com/Shirhe-Lyh/Xception>.

# Appendices

We first provide the link to the repository for our implementation of DCLS. We then give additional details on the architectures and source code we used to conduct our experiments namely: the ConvMixer architecture [12] and Deeplabv3+ [13]. Finally, we provide some additional results on the Imagenette dataset [17], which is a 10 class-subset of ImageNet1k [18], using ConvMixer with DCLS depthwise convolutions. Qualitative results on Pascal Voc 2012 dataset [19] are available as well.

## Appendix A: Repositories and reproducibility

The following repositories should be used to reproduce all the experiments presented in the article.

### DCLS

The main repository of the DCLS method is available at <https://github.com/K-H-Ismail/Dilated-Convolution-with-Learnable-Spacings-PyTorch>. It is based on Pytorch and CUDA. The code has been tested for CUDA 11 versions and versions of torch $\geq$ 1.5.0. We do not guarantee backward compatibility.

The installation could be done either by compiling the source code or by installing the provided package wheel. Please follow the instructions in the `README.md` file to install and use DCLS.

### ConvMixer

To reproduce the results provided in Section 6.2 please refer to the repository available at <https://github.com/K-H-Ismail/convmixer>. This is a fork of [20] developed by the authors of [12], we built on top of it to experiment DCLS. Training logs for baselines and models containing DCLS are also provided.

Please follow the instructions in the `README.md` file to get started.

### Deeplabv3+

To reproduce the results provided in Section 6.3 please refer to the repository available at <https://github.com/K-H-Ismail/DeepLabV3Plus-Pytorch>. This is a fork of [21], we built on top of it to experiment DCLS. We added the Xception65 backbone baseline by using the official Deeplab pretrained models available at [https://github.com/tensorflow/models/blob/master/research/deeplab/g3doc/model\\_zoo.md](https://github.com/tensorflow/models/blob/master/research/deeplab/g3doc/model_zoo.md). Those models were made for TensorFlow. However, we made the conversion to Pytorch using [22]. Checkpoints for baselines and models containing DCLS are available as well.

Please follow the instructions provided in the `README.md` file to get started.

## Appendix B: Additional details on architectures

In the following, we illustrate the architectures used to conduct the two experiments of the main article and modifications made to add DCLS modules.

### ConvMixer architecture

The ConvMixer architecture [12] is mainly based on convolutional layers. A patch embedding using a strided convolution (with stride factor equal to kernel size) is applied in the beginning, then a series of depthwise separable convolutions is applied before a global average pooling and a fully connected layer to get the predicted class. Figure 4 summarizes the described architecture.

In the CIFAR-10 experiment, we used a ConvMixer256/16 (width  $w = 256$  and depth  $d = 16$ ) model in which we replaced the depthwise  $9 \times 9$  convolutions by depthwise  $3 \times 3$  DCLS-2D convolutions with a maximum dilation rate of 3 as depicted in Figure 5.

In the additional Imagenette experiment (see Table 3), we used a ConvMixer1536/20 (width  $w = 1536$  and depth  $d = 20$ ) model where we also replaced the depthwise  $9 \times 9$  convolutions by depthwise  $3 \times 3$  DCLS-2D convolutions with a maximum dilation rate of 3.

### Deeplabv3+

The Deeplabv3+ architecture [13] is an extension of previous versions of Deeplab [16]. It consists of an encoder and a decoder part. The encoder part uses the low level features provided by the output of a pretrained backbone (Resnet, Mobilenet or Xception) and passes them to an Atrous Spatial Pyramid Pooling (ASPP) [13]. The outputs of the ASPP module are then interpolated and projected using a  $1 \times 1$  convolution. Both backbone and encoder outputs are used in the decoder part where a last convolution and an upsampling are made. Figure 6 summarizes the described architecture.

In the Deeplabv3+ experiment, we used different backbones for Deeplabv3+'s model and we replaced the three dilated convolutions used in the ASPP module by DCLS-2D convolutions with maximum dilation rates of 6, 12 and 18 as depicted in Figure 7.

## Appendix C: Additional Experiments

The additional experiments were carried out on the Imagenette dataset [17] as well as on the qualitative results of Deeplabv3+ model on the Pascal Voc 2012 validation dataset [19].

### Imagenette results

We reconduct the same CIFAR-10 experiment described in the Section 6.2 but now with the Imagenette dataset [17] which is a 10-class subset of ImageNet1k [18]. This experiment gives a good insight on what the results might be on the ImageNet1K dataset. We can see that the same observations made on the CIFAR-10 experiment hold for this one as well.

From Table 3, we can see that the 2D-DCLS convolution provides better Top-1 accuracy than both standard di-

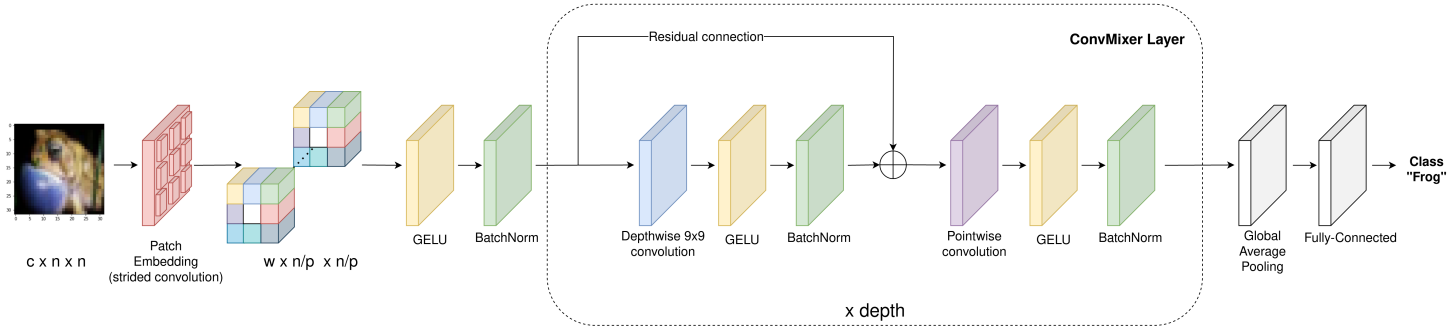


Fig. 4. Original ConvMixer architecture [12].

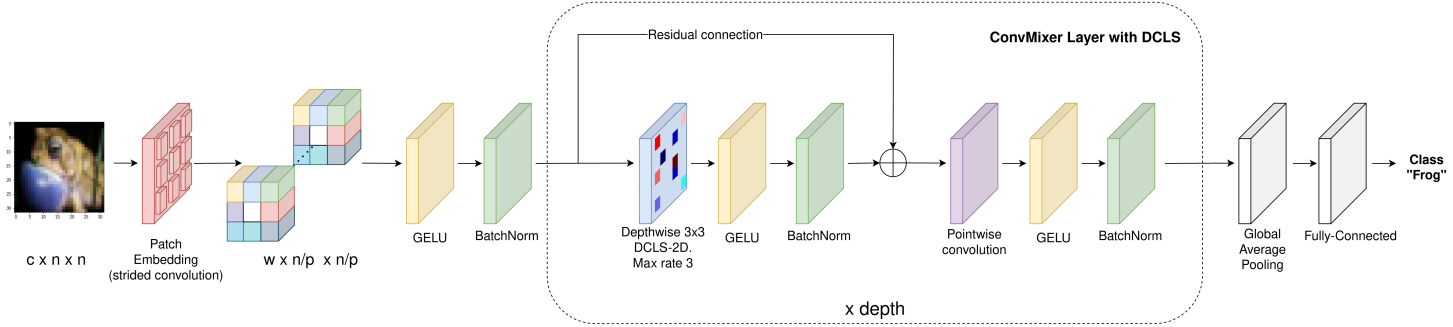


Fig. 5. ConvMixer with depthwise DCLS architecture.

ConvMixer trained on Imagenette [17] (a 10-class subset of ImageNet1k).

Width $w$	Depth $d$	Patch Size $p$	Kernel Size $k$	Dilation $d$	Scaling gain	# Params $\times (10^6)$	Method	Top-1 Acc. (%)
1536	20	7	9	1	-	50.10	Conv2d	94.67
1536	20	7	7	1	-	49.12	Conv2d	94.39
1536	20	7	3	1	-	47.89	Conv2d	93.27
1536	20	7	3	3	-	47.89	Conv2d	91.97
1536	20	7	3	3	$\frac{1}{k\sqrt{w}} \approx 0.008$	<b>48.44</b>	Dcls2d	<b>94.11</b>
1536	20	7	3	3	$\frac{10}{k\sqrt{w}} \approx 0.085$	<b>48.44</b>	Dcls2d	<b>94.34</b>

Table 3. Top-1 accuracies on Imagenette [17] (a 10 classes subset of ImageNet1k) trained exactly as in [12].

lated convolution (by +2.37%) and non dilated convolution (by +1.07%) and that with 1.14% more parameters. Moreover, it reaches slightly lower accuracy than the baseline (by -0.33%) and that with 3.32% less parameters. The standard dilated convolution achieves much lower performance than DCLS here also.

### Qualitative results on Pascal Voc 2012 validation set

Tables 4, 5 and 6 provide qualitative image segmentation on Pascal Voc 2012 validation set [19]. We have randomly chosen a few images that show a noticeable difference between DCLS and standard dilated convolution. The backbone used here is the Xception65 backbone pretrained on ImageNet [18] and COCO [14] datasets.

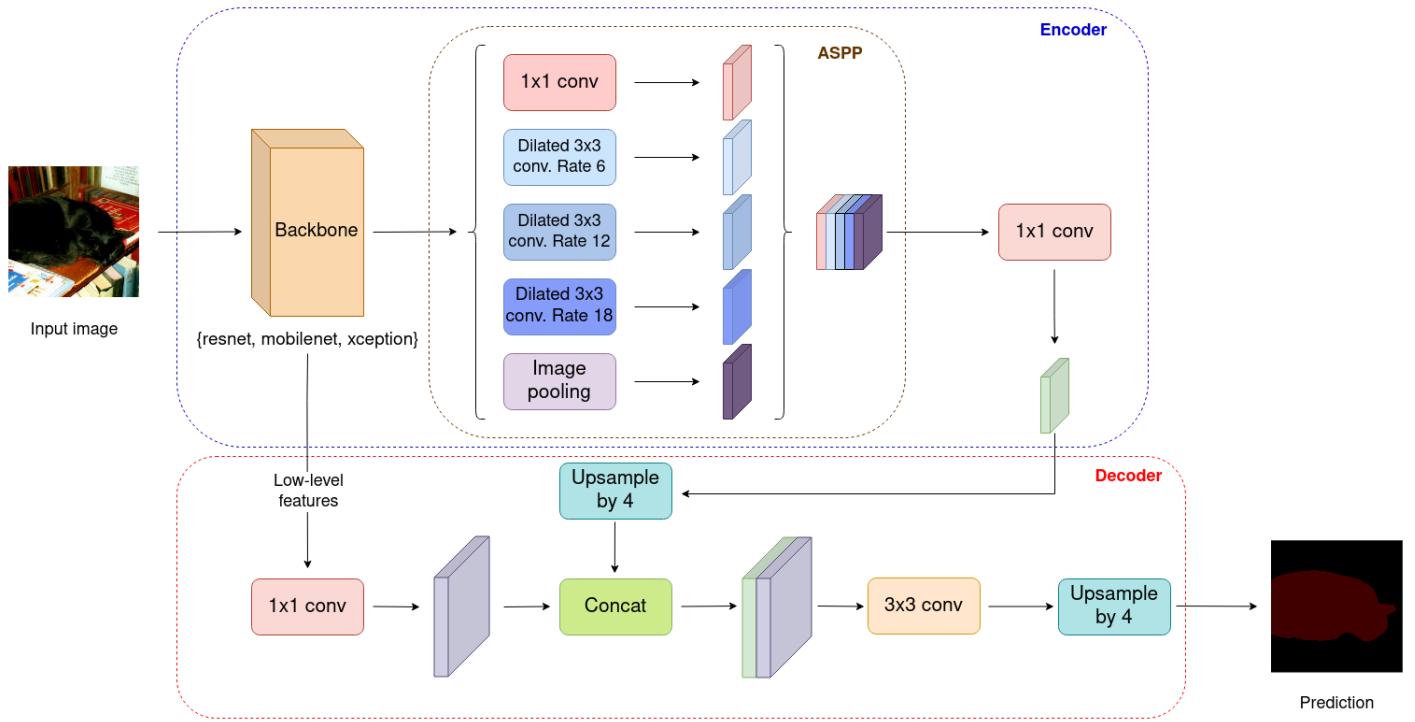


Fig. 6. Original Deeplabv3+ architecture [13].

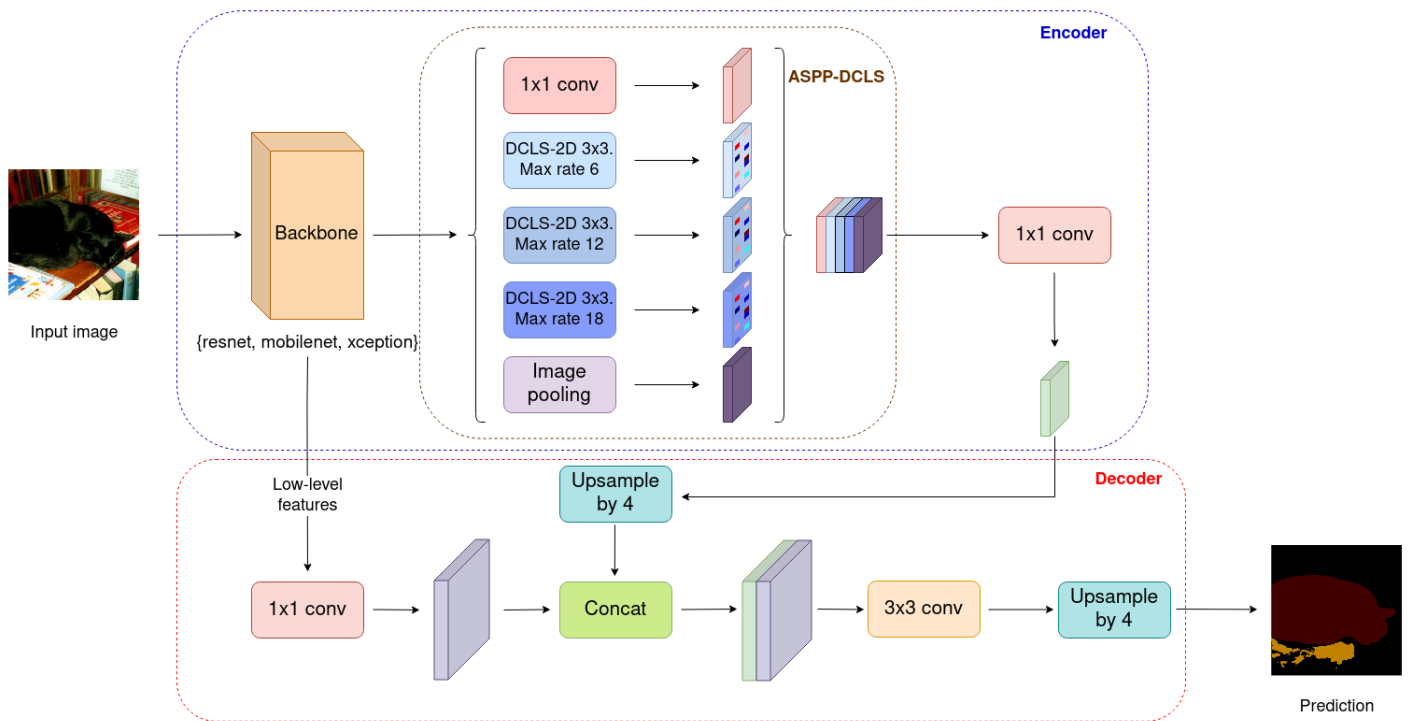


Fig. 7. Deeplabv3+ with DCLS ASPP architecture.

Original image	Ground truth	Baseline overlay	Baseline prediction	DCLS overlay	DCLS prediction

Table 4. Qualitative results on Pascal Voc 2012 validation set using Xception65 backbone.

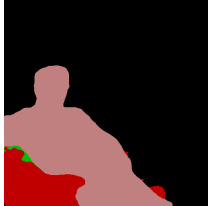
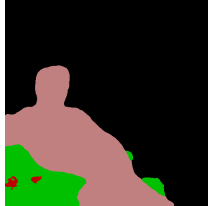
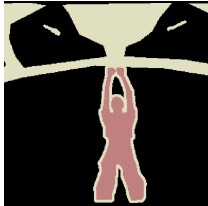
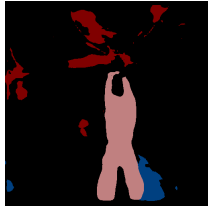
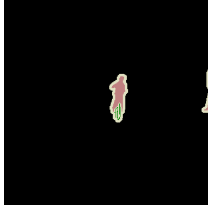
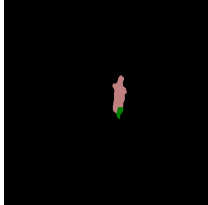
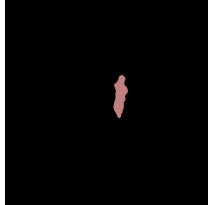
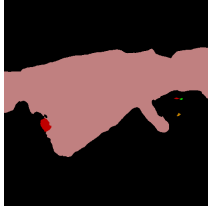
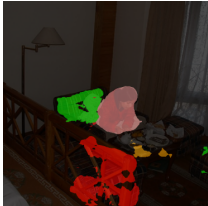
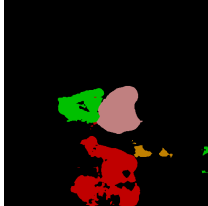
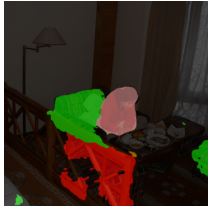
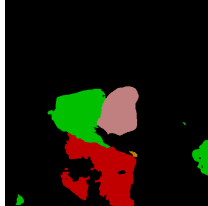
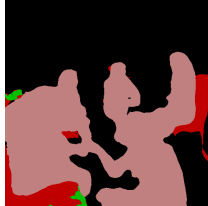
Original image	Ground truth	Baseline overlay	Baseline prediction	DCLS overlay	DCLS prediction
					
					
					
					
					
					
					
					

Table 5. Qualitative results on Pascal Voc 2012 validation set using Xception65 backbone.

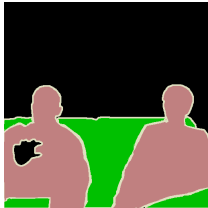
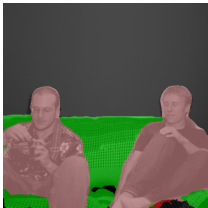
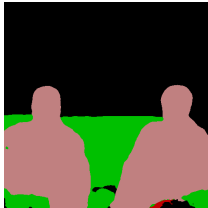
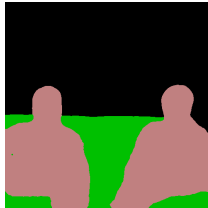
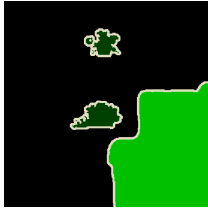
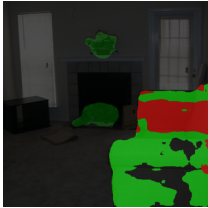
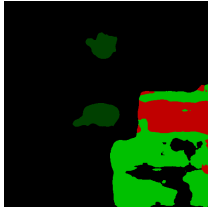
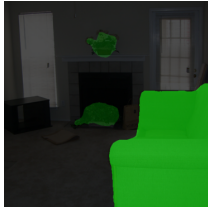
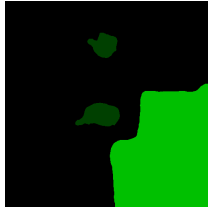
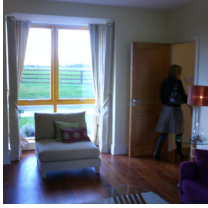
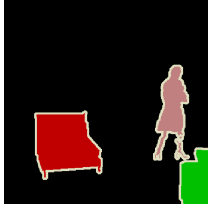
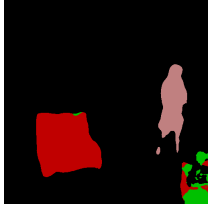
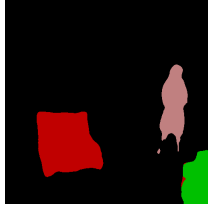
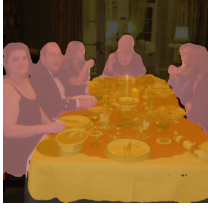
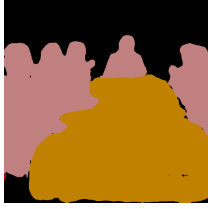
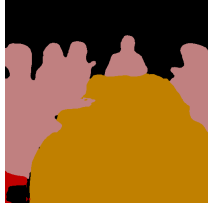
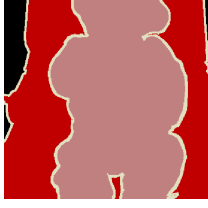
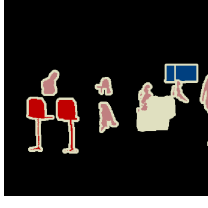
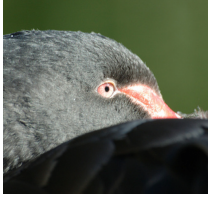
Original image	Ground truth	Baseline overlay	Baseline prediction	DCLS overlay	DCLS prediction
					
					
					
					
					
					
					
					

Table 6. Qualitative results on Pascal Voc 2012 validation set using Xception65 backbone.